IEEE Access
Multidisciplinary | Rapid Review | Open Access Journal

Received December 14, 2020, accepted January 4, 2021, date of publication January 8, 2021, date of current version January 19, 2021.

Digital Object Identifier 10.1109/ACCESS.2021.3050191

DC-Link Voltage Research of Photovoltaic Grid-Connected Inverter Using Improved Active Disturbance Rejection Control

XUESONG ZHOU, QIAN LIU, YOUJIE MA, AND BINGJIE XIE

Tianjin Key Laboratory for Control Theory and Applications in Complicated Industry Systems, School of Electrical and Electronic Engineering, Tianjin University of Technology, Tianjin 300384, China

Corresponding authors: Qian Liu (193125301@stud.tjut.edu.cn) and Youjie Ma (zxsmyj@126.com)

This work was supported in part by the National Natural Science foundation of China under Grant 51877152, and in part by the Natural Science Foundation of Tianjin of China under Grant 18JCZDJC97300.

ABSTRACT In this paper, a robust DC-link voltage control scheme is proposed to improve the tolerance of photovoltaic (PV) grid-connected inverter to disturbances. The sensitive characteristic of the DC-link voltage complicates the dynamics of the inverter control system and limits its overall performance, especially when uncertain disturbances are considered. To cope with this issue, a voltage controller based on the linear active disturbance rejection control (LADRC) is designed. By exploring the principle of deviation regulation, an improved linear extended state observer (LESO) is established to ensure that the total disturbance can be estimated in a relatively timely manner. The linear state error feedback (LSEF) control law is generated to compensate for the total disturbance, which reduces the plant to approximate the canonical cascaded double integrator. The stability and disturbance rejection capability of the improved LADRC are further analyzed in frequency domain. Finally, theoretical analysis and experimental results confirm the feasibility of the proposed control scheme.

INDEX TERMS Photovoltaic (PV) grid-connected inverter, DC-link voltage, linear active disturbance rejection control (LADRC), deviation regulation, total disturbance.

I. INTRODUCTION

In recent years, with the increasing depletion of traditional energy sources, renewable energy power generation has become the mainstream of industrial applications. Given the strategic position of solar energy in the global power energy structure, photovoltaic (PV) is expected to become the primary energy supply in the future, which has attracted increasing attention [1]–[4]. For the widely used two-stage PV grid-connected system, in addition to realizing maximum power point tracking (MPPT) and controlling the grid-connected current, the voltage across the DC-link capacitor connected to the front and rear stages must also be controlled within a reasonable range [2], [5]. Note that the DC-link voltage is prone to fluctuations due to active power disturbances. If it is not controlled correctly, the related protection system will be triggered.

Generally speaking, the DC-link voltage is regulated by the rear stage inverter control system, which usually adopts a dual-loop proportional-integral (PI) control structure. The outer voltage loop is responsible for keeping the DC-link voltage constant, while the inner current loop performs power factor correction and harmonic compensation on the gird side [6]–[8]. In the practice of PV grid connection, the presence of external disturbances (such as grid sag and environmental variations) makes it difficult for traditional PI control to achieve the desired performance [9]. Therefore, it is meaningful to conceive a robust voltage control scheme to enhance dynamics. In [10], a DC power control strategy has been proposed, which solves the negative impact of the severe fluctuation of the grid voltage on the DC-link voltage. However, the experimental results show that this method is not suitable for three-phase grid voltage unbalanced systems. Reference [11] proposed a method of adding feedforward control to voltage control loop by measuring load power. Nevertheless, this method puts forward high requirements for additional sensors. A sliding mode variable structure control

The associate editor coordinating the review of this manuscript and approving it for publication was Zhouyang Ren.

scheme is proposed in [12] to improve the robustness of the DC-link voltage. This strategy, however, needs to provide the parameter of the load resistance, which is undesirable from the practicality. Besides, [13] added a single-input space vector controller to the traditional PI regulator, which reduces the grid-side harmonic content and the ripple of the DC-link voltage, but the tuning process is too complicated.

Disturbance and uncertainty inherent in the plants require the design of robust controllers [14]–[18]. Besides, the essence of control is how to suppress undesirable disturbances. If the various disturbances in the control system are integrated into one category, just like the idea of disturbance observer (DoB) [15] and extended state observer (ESO) [16], it will be more convenient to design the controller. However, the observer and its resulting control system based on the plant model are sensitive to the deviation of the parameters, presenting certain limitations. ESO, which is widely used to estimate disturbances, does not dependent on the model information of the plant, compared with DoB [17]. ESO was initially proposed by Han in active disturbance rejection control (ADRC) [18], which can also work independently with other controllers. ADRC takes the cascaded integrator as the canonical form and regards the discrepancy between the system dynamics and the canonical form as the generalized disturbance (including various uncertainties and external disturbances) that can be estimated by ESO in real time. In order to facilitate the design and implementation, linear ADRC (LADRC) was proposed in [19], which introduced the concept of ''bandwidth'' into the control algorithm through pole configuration technology. Since then, theoretical analysis related to LADRC has been gradually carried out. In [20]–[25], the performance of LADRC-based systems, such as tracking, stability, and disturbance rejection capabilities, were investigated profoundly in both the time domain and the frequency domain.

The application of LADRC in the industry is eye-catching, which is mainly manifested in its strong tolerance to disturbance. In [26], a robust active damping method based on LADRC was proposed to improve the performance of an inverter connected to the grid through an inductor-capacitor-inductance (LCL) filter. In [27], cascaded linear ESO (LESO) was applied to interior permanent magnet synchronous motor (IPMSM). Experimental results indicated that the cascaded LESO could reconstruct slope-type disturbances with zero error, and the speed response is stable and without offset during the entire loading process. In another work [28], a secondary frequency control strategy for isolated microgrids based on LADRC strategy was proposed, which significantly suppresses frequency oscillations and has a faster response speed after adding demand response.

In this paper, an improved LADRC-based DC-link voltage controller is proposed for the PV grid-connected system, which is dedicated to enhancing the robustness when disturbed. The idea of improvement is inspired by the principle of deviation regulation in classical control theory. The remainder of this paper is organized as follows: Section II reveals the stability problem of the DC-link under disturbance conditions and conducts modeling and analysis on its dynamics. In Sections III and IV, the design process and characteristic analysis of the improved LADRC are investigated. Section V presents the experimental results, which validate the feasibility and effectiveness of the proposed control strategy with a 3-kW PV experimental platform. Finally, concluding remarks are drawn in Section VI.

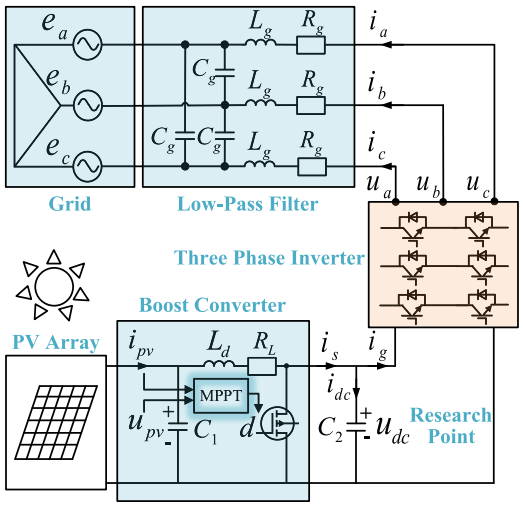

FIGURE 1. Schematic of two-stage PV grid-connected system structure.

TABLE 1. Inverter system parameters.

Symbol	Quantity	Value
f	Grid frequency	50 Hz
f_{sw}	Sampling frequency	10 kHz
u_{dc}	DC-link voltage	700 V
C_2	DC-link capacitance	2200 μF
R_g	Grid side filter resistance	0.1 Ω
C_g	Grid side filter capacitance	10 μF
L_g	Grid side filter inductance	10 mH

II. STABILITY PROBLEM AND DYNAMIC MODELING OF DC-LINK

Before starting the LADRC-based control strategy design, the DC-link under study is described and modeled.

A. DESCRIPTION OF DC-LINK STABILITY PROBLEM

The circuit topology of the two-stage PV grid-connected system is illustrated in Fig. 1. The front stage is connected to both ends of the DC-link capacitor via a boost circuit, realizing MPPT control. The rear stage, whose primary objective is to achieve the active power balance and grid connection, comprises a three-phase voltage source inverter, a low-pass filter, and the grid [7]. The inverter system parameters used in this study are listed in Table 1.

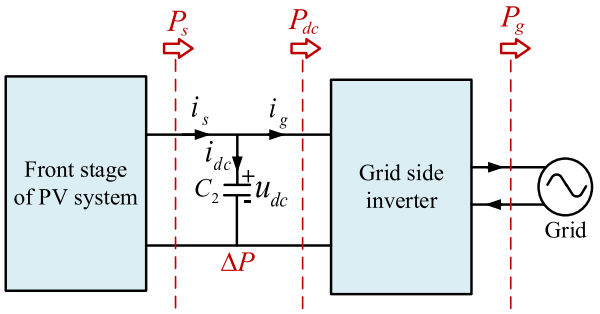

FIGURE 2. Description of the power relationship between the DC-link and the grid.

Modeling the grid-connected inverter in the three-phase static coordinate system gives

$$\begin{bmatrix} u_a \\ u_b \\ u_c \end{bmatrix} = L\frac{d}{dt}\begin{bmatrix} i_a \\ i_b \\ i_c \end{bmatrix} + R\begin{bmatrix} i_a \\ i_b \\ i_c \end{bmatrix} + \begin{bmatrix} e_a \\ e_b \\ e_c \end{bmatrix} \tag{1}$$

where u_x, i_x and e_x respectively represent the inverter output phase voltage, grid current, and grid phase voltage ($x = a, b, c$). Transform (1) into the dq coordinate system rotating synchronously with the grid angular frequency through Park transformation, simplifying the design of the control system.

$$\begin{bmatrix} u_d \\ u_q \end{bmatrix} = L\frac{d}{dt}\begin{bmatrix} i_d \\ i_q \end{bmatrix} + R\begin{bmatrix} i_d \\ i_q \end{bmatrix} + \begin{bmatrix} e_d \\ e_q \end{bmatrix} + \omega L\begin{bmatrix} -i_q \\ i_d \end{bmatrix} \tag{2}$$

where $u_{(dq)}$, $i_{(dq)}$, and $e_{(dq)}$ are the dq-axis components corresponding to the variables in (1). ω indicates the grid nominal angular frequency.

In order to realize the separate control of active power and reactive power on the grid side, a vector control method based on grid voltage orientation is usually adopted. In the dq reference frame, aligning the d-axis direction with the grid voltage vector E, then $e_d = |E|, e_q = 0$. $|E|$ represents the peak value of the phase voltage of the grid, which is 311V in this paper. Therefore, the active power and reactive power injected into the grid by the inverter can be described by the instantaneous power theory as [29]:

$$\begin{cases} P_g = 3e_d i_d/2 \\ Q_g = -3e_d i_q/2 \end{cases} \tag{3}$$

Fig. 2 reveals the dynamic power balance relationship between the DC-link and the grid, which can be expressed as:

$$\begin{aligned} i_{dc} &= i_s - i_g = C_2\frac{du_{dc}}{dt} \\ P_s - P_{dc} &= u_{dc}i_{dc} = \Delta P \\ P_{dc} &= P_g \end{aligned} \tag{4}$$

where i_s, i_g, and i_{dc} are the output current of the front stage, the input current of the rear stage, and the current flowing into the DC-link capacitor. If the power loss of the AC side filter and switching devices is not considered, the inverter DC side terminal power P_{dc} is equal to the grid side power P_g.

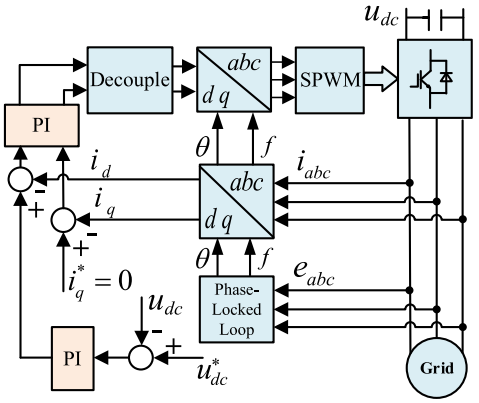

FIGURE 3. Schematic of a grid-connected inverter system with the commonly adopted control structure.

During the steady-state operation of the grid-connected system, the front and rear power levels are balanced with $P_s = P_{dc}$, and DC-link voltage is constant at the nominal value. When encountering unexpected disturbances, such as variations in cell temperature, solar irradiance, and grid voltage, this balance will be instantly broken. Taking the grid voltage sag as an example, the active power consumed by the grid side will decrease. In the short term, the active power P_s output by the front stage cannot be completely transmitted to the grid, resulting in excess power to accumulate in the capacitor with $\Delta P > 0$. Then the DC-link voltage will rise, driving the current flowing through the capacitor to increase rapidly [5], [8]. If not handled in time, excessive voltage and current will break down the DC-link capacitor and affect the operation of other equipment.

Therefore, strong robustness against unknown disturbances must be a key attribute in DC-link voltage control to guarantee the regular operation of the system.

B. DYNAMIC MODEL OF DC-LINK VOLTAGE LOOP

Equation (3) illustrates the principle of the current inner loop, which is that the grid-side power can be controlled through the dq-axis current. A grid-connected inverter system with its commonly adopted control structure is described in Fig. 3. The reference frequency and phase for performing Park transformation are provided by a phase-locked loop, which samples the grid voltage [11]. The input of the outer loop controller is the DC-link voltage reference u_{dc}^*, and the output is the d-axis reference current i_d^*. For the inner loop controller, in order to achieve unity power factor control, set the q-axis current reference $i_q^* = 0$. Finally, after the current is decoupled, the inverse coordinate transformation is performed to obtain the modulation signal to drive the sinusoidal pulse width modulation (SPWM) module.

Supposing that the DC-link voltage is already in a steady state and well controlled ($u_{dc} = u_{dc}^*$). Under this premise, the relationship between i_s and i_d can be given by

$$u_{dc}^* i_s = 3e_d i_d/2 \tag{5}$$

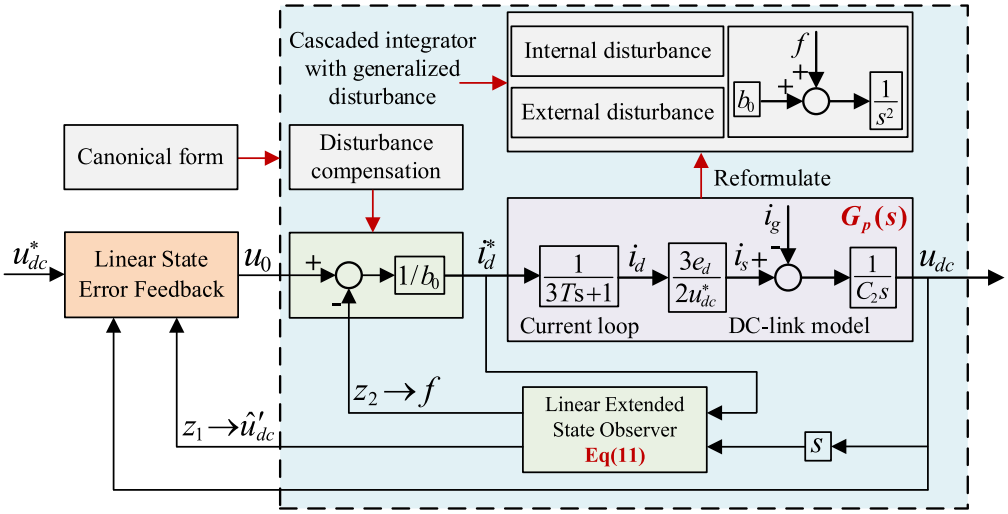

FIGURE 4. LADRC-based DC-link voltage control diagram.

Therefore, the dynamic model (4) can be rewritten as:

$$C_2\frac{du_{dc}}{dt}=\frac{3e_d i_d}{2u_{dc}^*}-i_g \tag{6}$$

Equation (6) implies that the DC-link voltage control can be achieved by controlling the d-axis component of the grid current.

Using the PI control parameter configuration method of the inner loop in [30], the d-axis current transfer function can be approximated to an inertial link, $1/(3Ts+1)$. Considering this fact, the LADRC-based voltage outer loop control block diagram is given in Fig. 4, where $G_p=\frac{3e_d}{2u_{dc}^*C_2s(3Ts+1)}$ can be regarded as a second-order controlled plant with external disturbance i_g. If the DC-link voltage is not effectively controlled, the current loop will be negatively affected.

The research of this paper is carried out around the design of a robust voltage controller, which is introduced and analyzed in detail in Sections III and IV.

III. ROBUST DC-LINK VOLTAGE CONTROL SCHEME

It can be concluded from the above analysis that excellent disturbance rejection capability is one of the crucial characteristics that should be considered in the voltage controller for grid-connected applications. LADRC possesses the natural advantage of tolerating all uncertainties, which is mainly manifested by the ability to estimate and compensate for generalized disturbances accurately. As shown in Fig. 4, LADRC is composed of LESO and linear state error feedback (LSEF) control law. LESO expands the generalized disturbance in the system dynamics which is different from the canonical cascaded integrator into a new state variable to estimate. LSEF uses a classic proportional-derivative (PD) controller to synthesize the control signal u_0 required for disturbance compensation [19]–[21].

In this section, a voltage control strategy based on improved LADRC is designed according to the principle of deviation regulation, which can relatively reduce the fluctuation of DC-link voltage under disturbances while ensuring good tracking of the current reference.

A. THE IDEA OF IMPROVED LESO BASED ON DEVIATION REGULATION PRINCIPLE (D-LESO)

Consider the second-order controlled plant described by the voltage loop in Fig. 4.

$$\ddot{y}=-a_1\dot{y}-a_0y+bu+w \tag{7}$$

where $a_1=2/(3T), a_0=0, b=e_d/(2u_{dc}^*C_2T)$. w represents the external disturbance, including the injected current i_g, parametric uncertainties and unmodeled dynamics, etc. u is the manipulated input i_d^* of the plant; y is the output u_{dc}.

The first step before using LESO is to reformulate the plant with various disturbances into a canonical form of cascaded integrator with generalized disturbance. Then, the plant (7) can be rewritten as:

$$\ddot{y}=f(y,\dot{y},w,t)+b_0u \tag{8}$$

where f is denoted as the generalized disturbance or total disturbance, integrating the unknown external disturbance w and the known internal disturbance $-a_1\dot{y}-a_0y+(b-b_0)u$. b_0 represents a scaling factor that can be adjusted arbitrarily.

For a second-order voltage control system, a third-order LESO framework is usually used to estimate the total disturbance. However, when the DC-link voltage is measurable, a reduced-order LESO can be used to decrease the complexity of the algorithm and improve the rapidity of disturbance estimation. Therefore, $\dot{y}$ can be considered as the first state variable x_1, and f is considered as the augmented state x_2 [31]. Assuming that f is differentiable, the augmented state space model of the plant (8) can be constructed by

$$\begin{cases}\dot{x}=Ax+Bu+Eh\\ y=Cz\end{cases} \tag{9}$$

where $A = \begin{bmatrix} 0 & 1 \\ 0 & 0 \end{bmatrix}, B = \begin{bmatrix} b_0 \\ 0 \end{bmatrix}, C = \begin{bmatrix} 1 & 0 \end{bmatrix}, E = \begin{bmatrix} 0 \\ 1 \end{bmatrix}$, $h = \dot{f}$.

Based on the standard model (9), the corresponding LESO can be formulated as follows [32]:

$$\begin{cases} \dot{z} = Az + Bu + L(\dot{y} - \hat{y}) \\ \hat{f} = Vz \end{cases} \tag{10}$$

After simple mathematical calculations, (10) is rewritten as:

$$\begin{bmatrix} \dot{z}_1 \\ \dot{z}_2 \end{bmatrix} = \begin{bmatrix} -l_1 & 1 \\ -l_2 & 0 \end{bmatrix} \begin{bmatrix} z_1 \\ z_2 \end{bmatrix} + \begin{bmatrix} b_0 & l_1 \\ 0 & l_2 \end{bmatrix} \begin{bmatrix} u \\ \dot{y} \end{bmatrix}$$
$$\hat{f} = \begin{bmatrix} 0 & 1 \end{bmatrix} \begin{bmatrix} z_1 \\ z_2 \end{bmatrix} \tag{11}$$

where L represents the observer gain vector, which can be obtained by pole placement method. $\hat{f}$ is the estimated value of the total disturbance. z_1, z_2 closely track x_1 and x_2 respectively.

By defining the tracking error $e_1 = z_1 - x_1$, the framework of LESO can be reduced from (11) to

$$\begin{cases} \dot{z}_1 = -l_1 e_1 + z_2 + b_0 u \\ \dot{z}_2 = -l_2 e_1 \end{cases} \tag{12}$$

The regulatory mechanism of LESO revealed in (12) shows that the dynamic tracking of state variables is controlled by the negative feedback of the error e_1. Mapping this mechanism to the deviation regulation in classical control theory, we will find that the dynamic estimation process of the total disturbance is adjusted by the error of another state variable. Under this premise, the estimation of z_2 has a certain hysteresis compared with z_1. Secondly, when z_1 has achieved good tracking, the adjustment of z_2 will appear powerless, because e_1 presents a very small state at this time. In order to make up for the above shortcomings, the l_2 determined in the conventional LESO is an order of magnitude larger than l_1. But too large observation gain will degrade the noise immunity of the system. Therefore, from the analysis of the deviation control, the process of LESO estimates the total disturbance is more worthy of feedback adjustment through the error between z_2 and x_2.

From the above analysis, it can be seen that how to obtain the estimation error of the total disturbance is particularly important. After mathematical derivation, (12) can be transformed into

$$z_2 = (\dot{e}_1 + \dot{x}_1) + l_1 e_1 - b_0 u \tag{13}$$

Substituting $\dot{x}_1 = x_2 + b_0 u$ into (13) results in:

$$z_2 = l_1 e_1 + \dot{e}_1 + x_2 \tag{14}$$

Therefore, the disturbance estimation error can be defined as $l_1 e_1 + \dot{e}_1$. Using it as the control quantity of z_2 can accelerate the convergence speed of the observer. With this idea, D-LESO can be constructed as follows:

$$\begin{cases} \dot{z}_1 = -l_1 e_1 + z_2 + b_0 u \\ \dot{z}_2 = -l_2 e_2 \end{cases} \tag{15}$$

which can be written in the state space model:

$$\begin{bmatrix} \dot{z}_1 \\ \dot{z}_2 \end{bmatrix} = \begin{bmatrix} -l_1 & 1 \\ 0 & -l_2 \end{bmatrix} \begin{bmatrix} z_1 \\ z_2 \end{bmatrix} + \begin{bmatrix} b_0 & l_1 & 0 \\ -l_2 b_0 & 0 & l_2 \end{bmatrix} \begin{bmatrix} u \\ \dot{y} \\ \ddot{y} \end{bmatrix} \tag{16}$$

According to the pole configuration method, the observer gain vector L can be selected so that the eigenvalues of the D-LESO matrix are all at $-\omega_o$ [22]:

$$L = \begin{bmatrix} \omega_o & \omega_o \end{bmatrix}^T \tag{17}$$

where ω_o is referred to as the observation bandwidth. In practice, its determination reflects the trade-off between the speed of state reconstruction and noise immunity [21].

B. LSEF CONTROL LAW AND DISTURBANCE COMPENSATION LINK

With the well-tuned D-LESO, the dynamics of the total disturbance can be fully captured. To achieve the desired control goal, the disturbance compensation link given below needs to be combined:

$$u = \frac{u_0 - z_2}{b_0} \tag{18}$$

If the estimation error of z_2 is ignored, the plant (8) can be reduced to a unit gain double integrator,

$$\ddot{y} = (f - z_2) + u_0 \approx u_0 \tag{19}$$

which can be controlled by a PD controller without much effort [19]:

$$u_0 = k_p(v - y) - k_d z_1 \tag{20}$$

where v is the setpoint u_{dc}^* of the DC-link voltage. k_p and k_d are the parameters of the PD controller.

Note using $-k_d z_1$ instead of $k_d(\dot{v} - \dot{z}_1)$ to avoid the differentiation of the setpoint and make the closed-loop transfer function a standard second-order system without zeros:

$$G_{cl}(s) = \frac{k_p}{s^2 + k_d s + k_p} \tag{21}$$

Here, k_p and k_d can be selected as follows to prevent the system from oscillating when meeting a higher response speed.

$$k_p = \omega_c^2, \quad k_d = 2\omega_c \tag{22}$$

ω_c is referred to as the control bandwidth, which determines the response speed of the system.

In the parameter tuning process of LADRC, the control performance and noise immunity of the DC-link voltage need to be considered at the same time. For the relationship between the two bandwidths, a general rule of thumb is to choose: $\omega_o = 1 \sim 5\omega_c$ [25].

IV. CHARACTERISTIC ANALYSIS OF THE IMPROVED LADRC STRATEGY

This section compares the characteristics of the conventional LADRC and the improved one in the frequency domain. The expressions of the conventional LADRC used are listed in the Appendix.

A. DISTURBANCE ESTIMATION CAPABILITY ASSESSMENT

Being able to estimate state variables in time and accurately is what an excellent observer deserves. By applying Laplace transform to (16), the working mode of D-LESO can be described in the form of transfer function:

$$\begin{cases} z_1 = \dfrac{b_0 s u}{(s+\omega_o)^2} + \dfrac{(2s^2\omega_o + \omega_o^2 s)y}{(s+\omega_o)^2} \\ z_2 = \dfrac{-b_0\omega_0 u}{s+\omega_o} + \dfrac{s^2\omega_o y}{s+\omega_o} \end{cases} \tag{23}$$

Combined with (9), the estimation error can be calculated as:

$$\begin{cases} e_1 = \dfrac{b_0 s u - s^3 y}{(s+\omega_o)^2} \\ e_2 = \dfrac{b_0 s u - s^3 y}{s+\omega_o} \end{cases} \tag{24}$$

Considering the typicality of the analysis, select u, y as the step signal with amplitude K, described as $u(s) = K/s, y(s) = K/s$. Then the steady-state error can be obtained according to the final value theorem [25]:

$$\begin{cases} e_{1s} = \lim\limits_{s\to 0} s e_1 = 0 \\ e_{2s} = \lim\limits_{s\to 0} s e_2 = 0 \end{cases} \tag{25}$$

Obviously, the proposed D-LESO has good convergence and can realize the error-free estimation of state variables.

By substituting (8) into (23), the transfer function between the estimated value z_2 of the total disturbance and the actual value f can be derived,

$$\frac{z_2}{f} = \frac{\omega_o}{s+\omega_o} \tag{26}$$

which reflects the disturbance estimation ability of the observer. The frequency-domain Bode plots for disturbance estimation of conventional LESO and improved one are depicted in Fig. 5, with $\omega_o = 30(rad/s)$. It can be observed that the two observers behave like a low-pass filter for input disturbances. However, the amplitude gain of the D-LESO in the middle and high-frequency range is more considerable, and the phase is also advanced by 90°. This phenomenon indicates that D-LESO can better estimate specific types of high-frequency disturbances compared to conventional LESO.

In order to verify the above conclusions, the unknown disturbance of plant (7) is temporarily excluded, and the internal disturbance is regarded as the total disturbance. The curves for estimating the internal disturbance are depicted in Fig. 6, where in the framework of D-LESO, the estimated curve is more consistent with the actual one. Furthermore, the period for the controller to compensate for internal disturbances is also shortened by 0.07s. This excellent performance is attributed to the fact that D-LESO can provide the controller with disturbance information more quickly, accelerating the disturbance compensation process.

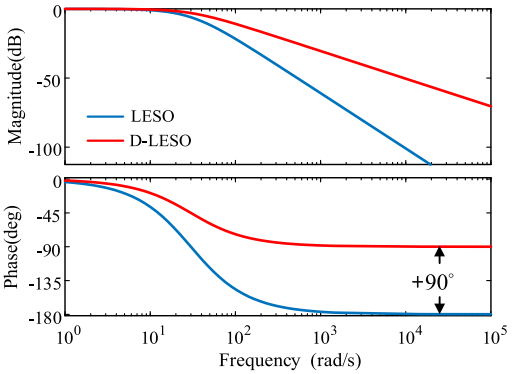

FIGURE 5. Bode plots for estimating the total disturbance.

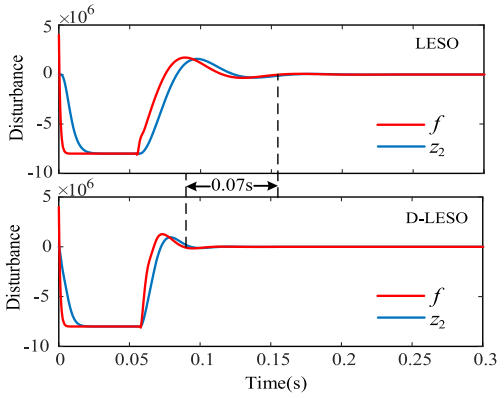

FIGURE 6. Time-domain curve for estimating internal disturbance.

B. DISTURBANCE REJECTION CAPABILITY ASSESSMENT

For a control system, from the perspective of practical application, the kernel of the control should be to suppress the disturbances and uncertainties in the process or system.

In the voltage control loop based on the improved LADRC, the control input i_d^* can be expressed by combining (18) and (20):

$$u = \frac{\omega_c^2(v-y) - 2\omega_c z_1 - z_2}{b_0} \tag{27}$$

In view of this, substituting (23) into (27) gives the following:

$$u = \frac{G_1(s)v - G_2(s)y}{H(s)} \tag{28}$$

where:

$$\begin{aligned} G_1(s) &= \omega_c^2(s+\omega_o)^2, \quad H(s) = b_0(s^2 + \omega_o s + 2\omega_c s) \\ G_2(s) &= \omega_o s^3 + (\omega_o^2 + \omega_c^2 + 4\omega_o\omega_c)s^2 \\ &\quad + (2\omega_c\omega_o^2 + 2\omega_c^2\omega_o)s + \omega_o^2\omega_c^2 \end{aligned}$$

By introducing the notation of (28), the voltage control loop based on the improved LADRC can be formulated to a two-degree-of-freedom (2dof) closed-loop system, as shown in Fig. 7. On this basis, the control loop has a standard structure of feedback and controlled plant [5]. The controlled plant is described as a canonical form to facilitate the analysis of the transfer function of the system output concerning the

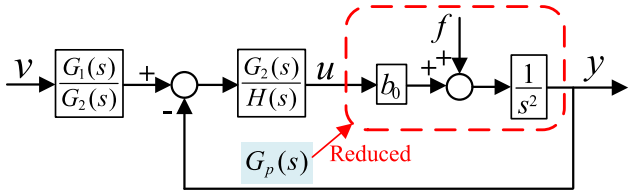

FIGURE 7. Implementation of an improved LADRC framework in the form of 2-dof.

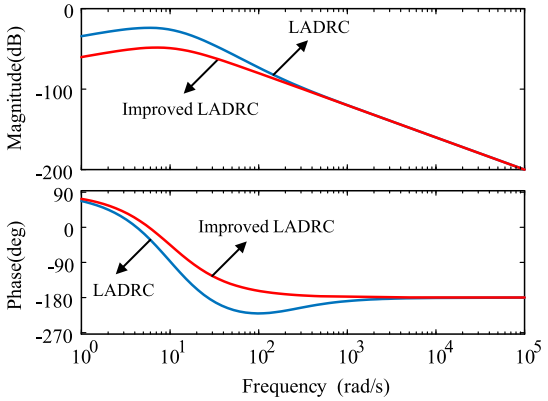

FIGURE 8. Bode plots for comparing disturbance term.

input and the total disturbance separately, which is given below:

$$y = \frac{b_0 G_1(s)v + H(s)f}{H(s)s^2 + b_0 G_2(s)} = \frac{\omega_c^2 v}{(s+\omega_c)^2} + \frac{s(s+2\omega_c+\omega_o)f}{(s+\omega_c)^2(s+\omega_o)^2} \tag{29}$$

The derivation of (29) proves that the control output consists of tracking term and disturbance term. If the disturbance can be correctly compensated, the transfer function is simplified to (21), which means that the system can track the setpoint quickly without overshoot.

How to enhance the tolerance to disturbance is the focus of this paper. Similarly, the Bode plots analysis is performed in the frequency-domain for the disturbance term of the conventional LADRC and the improved one. As shown in Fig. 8, the improved LADRC has a smaller amplitude gain and lower phase delay than the conventional LADRC in the mid-frequency range. However, in the high-frequency range, their amplitude-frequency characteristic curves overlap. At this time, the control performance of LADRC is mainly limited by the observation bandwidth of LESO [26].

Besides, the disturbance term with different bandwidths of improved LADRC is compared in Fig.9, where the amplitude gain gradually decreases as the bandwidth increases. It means that the higher the selected bandwidth, the more tolerant the system is to disturbances and uncertainties.

C. STABILITY ANALYSIS

The critical factor in evaluating the quality of a controller is the stability index, which can be tested by the Lienard-Chipart criterion. From Fig. 7, the transfer function of the voltage loop

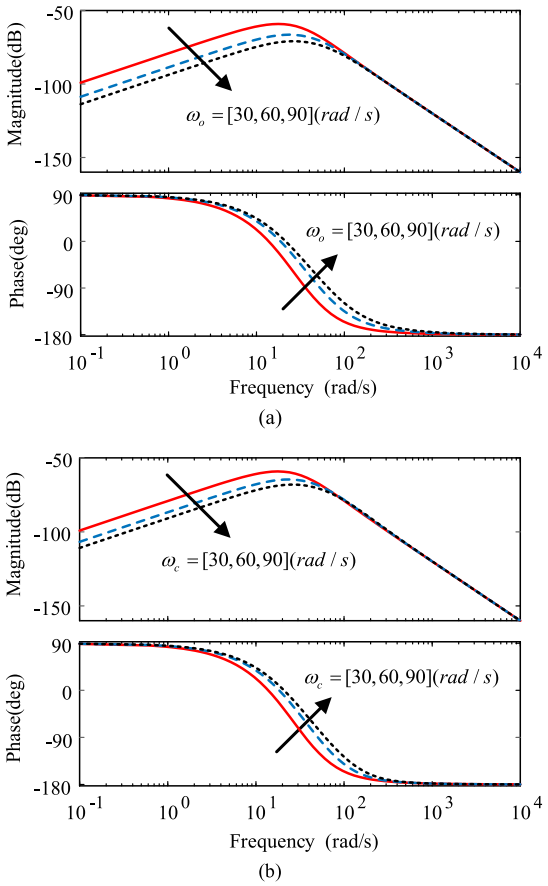

FIGURE 9. Bode plots of disturbance term with different bandwidths. (a) $\omega_c = 30(rad/s)$ (b) $\omega_o = 30(rad/s)$.

equipped with the improved LADRC can be readily available:

$$\frac{y}{v} = \frac{G_1(s)G_p(s)}{H(s) + G_2(s)G_p(s)} \tag{30}$$

The stability of the closed-loop system can be determined from the poles of (30), whose characteristic polynomial is:

$$p(s) = p_0 s^4 + p_1 s^3 + p_2 s^2 + p_3 s + p_4 \tag{31}$$

where the coefficients in (31) are listed in the Appendix. Since ω_o, ω_c, b and the system parameters in Table 1 are all positive, it can be concluded that $p_i > 0$, $(i = 0, 1, 2, 3, 4)$. On this basis, according to the Lienard-Chipart criterion, the necessary and sufficient condition for the stability of the control system is that all odd-order Hurwitz determinants are positive:

$$\Delta_1 > 0, \quad \Delta_3 > 0 \tag{32}$$

After calculating by Mathematic software, the following relationship can be derived:

$$\Delta_1 = p_1 > 0, \quad \Delta_3 = \begin{vmatrix} p_1 & p_3 & 0 \\ p_0 & p_2 & p_4 \\ 0 & p_1 & p_3 \end{vmatrix} > 0 \tag{33}$$

which proves that the voltage control system designed in this paper has good stability.

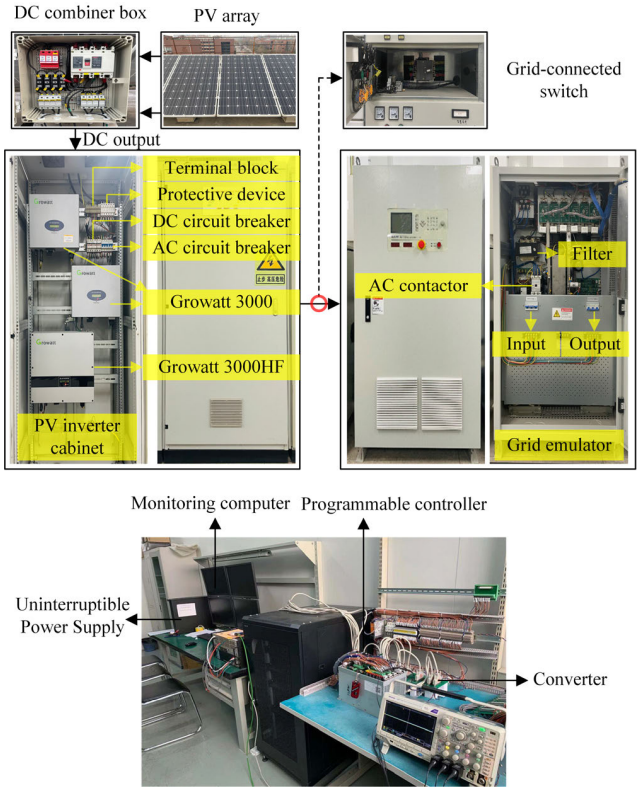

FIGURE 10. Experimental setup.

V. EXPERIMENTAL RESULTS

A 3-kW PV grid-connected experimental platform has been built to verify the feasibility of the proposed control strategy, as shown in Fig 10. The PV array consists of thirteen monocrystalline silicon solar panels connected in series. Under standard testing condition, the open-circuit voltage and maximum power point voltage of each panel are 36.5V and 29.1V, respectively. The short-circuit current and the maximum power point current are 9.1A and 8.42A. The PV array is connected in parallel with the combiner box to transmit the generated DC current to the inverter. The combiner box can reduce the wiring between the PV array and the inverter. Besides, the connection between the inverter and the grid emulator with phase voltage peak value of 311V is controlled by grid-connected switch device. The inverter tested in the experiment is divided into Growatt 3000 and Growatt 3000F, and its switching frequency and sampling frequency are both 10kHz.

Because this paper focuses on the optimization of the outer voltage loop, the verification of the proposed strategy is mainly realized by analyzing the control effect of DC-link voltage. For a fair comparison, the same parameters are configured for the conventional LADRC and the improved one, which are $\omega_c = 118(rad/s), \omega_o = 590(rad/s)$, and $b_0 = 17000$. Besides, the PI control parameters are selected by combining the optimal pole placement method in [30], which can guarantee a good trade-off between tracking and disturbance rejection.

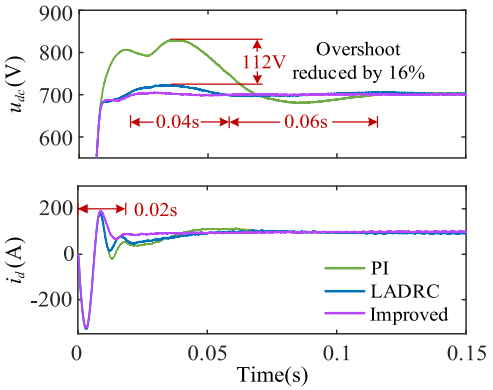

FIGURE 11. Time-domain behavior of the startup process under nominal working conditions ($S = 1000W/m^2$, $T = 25\,°C$).

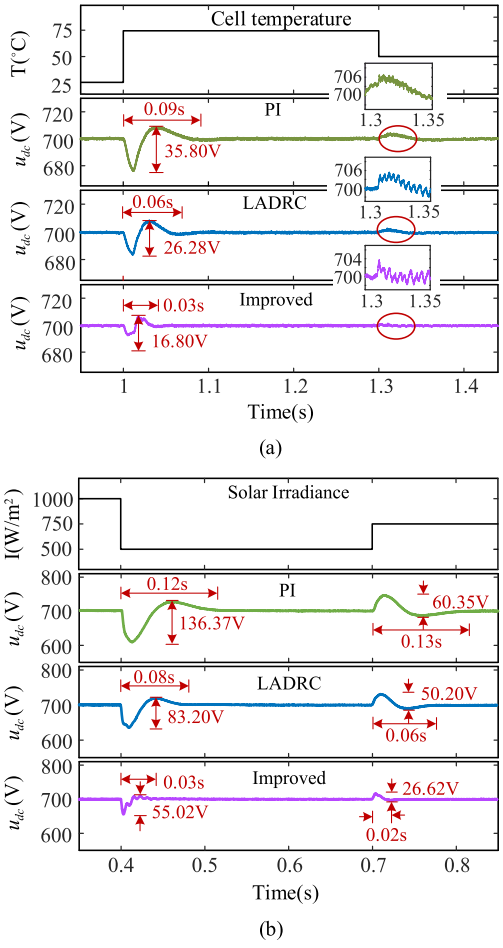

FIGURE 12. Time-domain behavior of DC-link voltage under step disturbances. (a) Step variations in cell temperature. (b) Step variations in solar irradiance.

The control performance analysis of the DC-link voltage is based on the following three cases:

Case 1: Nominal operating conditions.

Case 2: Step variations in cell temperature and solar irradiance.

Case 3: Voltage sags of varying degrees on the grid.

A TMS320F28335 DSP is used as the processor of the PV grid-connected inverter control system. Import the

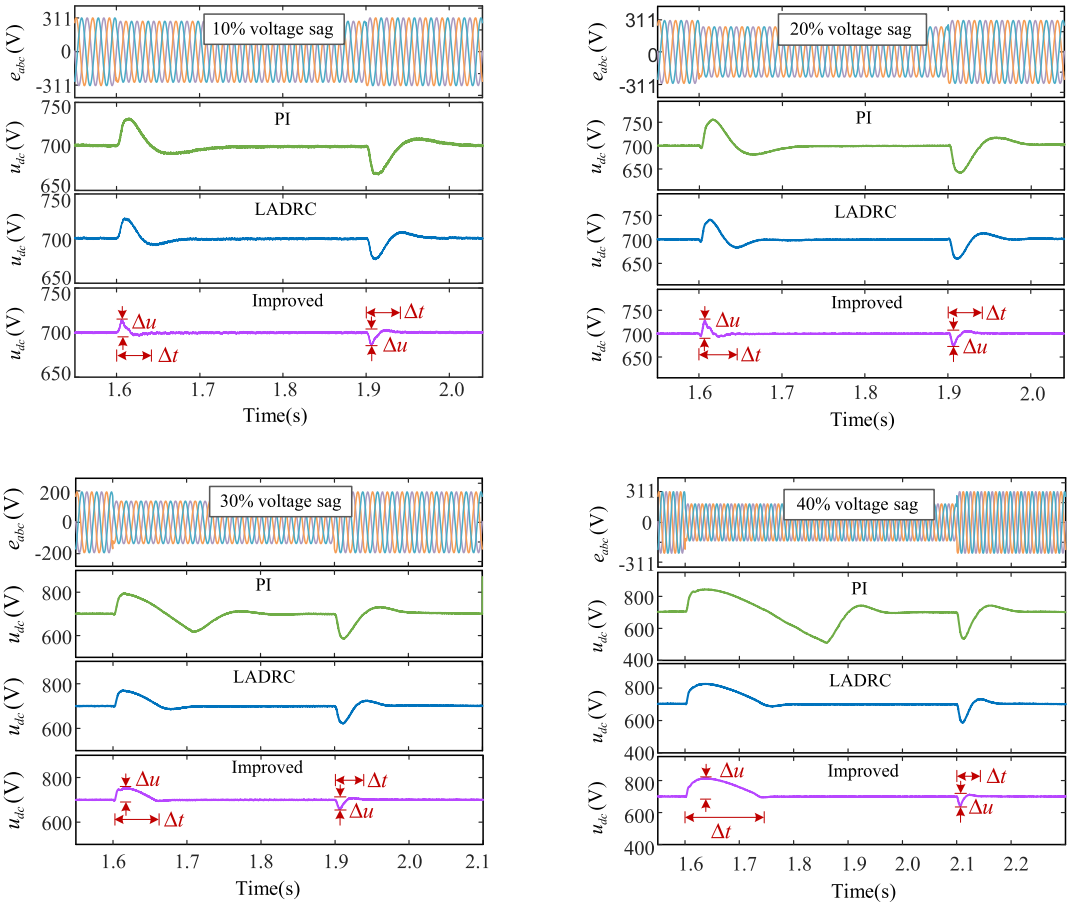

FIGURE 13. Time-domain behavior of DC-link voltage under the condition of grid voltage sag, the fluctuation range of the DC-link voltage is denoted as Δu, and the recovery time is denoted as Δt.

experimental result data into MATLAB/Simulink for curve fitting and analysis.

A. SET-POINT TRACKING PERFORMANCE

In PV grid-connected system, the typical characteristics of dual-loop control determine that the performance of grid-side current is restricted by the DC-link voltage. With this in mind, a comparative experiment was performed on the DC-link voltage and d-axis current under nominal operating conditions to analyze the tracking performance of the set-point.

Theoretically speaking, the advantage of LADRC over PI control is that its response speed and overshoot are not contradictory under ideal conditions. As presented in Fig. 11, LADRC reduces the overshoot by 16% while shortening the settling time by 0.06s, compared to PI control. In fact, the voltage overshoot under LADRC is essentially caused by insufficient disturbance compensation, which can be known from (29). For the proposed improved LADRC, the timely estimation of the observer lays the cornerstone for eliminating the total disturbance, thereby weakening the negative effect of the disturbance term. Therefore, the improved LADRC avoids the generation of voltage overshoot and completes the transition process 0.04s earlier than the conventional one.

The balance of the DC-link voltage provides a stable reference command for the d-axis current. Correspondingly, when using the improved LADRC voltage controller, the d-axis current can track the set point faster within 0.02s.

In summary, the PV grid-connected inverter based on the improved LADRC possesses better tracking performance during system startup, which can be attributed to the strong disturbance estimation capability of D-LESO.

B. ROBUSTNESS UNDER STEP VARIATIONS OF CELL TEMPERATURE AND SOLAR IRRADIANCE

Affected by the environment, the battery temperature and solar irradiance will inevitably change, resulting in DC-link voltage fluctuations. This investigation is implemented to evaluate and compare the robustness of the three control algorithms under the condition of cell temperature and solar irradiance step variations.

As can be observed from Fig. 12(a), when the PV panel undergoes a 50-degree step variation under nominal operating conditions, the employment of the conventional LADRC significantly improves the capability of rejecting disturbance, with voltage fluctuation reduced to the half and recovery time shortened to two-thirds, compared with PI control. However, the improved LADRC exhibits better dynamic performance

with a voltage undershoot of 16.80V and a recovery time of 0.03s. Also, when the cell temperature drops by 25 degrees at 1.3s, the improved LADRC can basically maintain the DC-link voltage balance, which demonstrates a higher tolerance for temperature disturbance.

On the other hand, Fig. 12(b) illustrates the experimental results of the DC-link voltage under step variations in solar irradiance. Similar to Fig. 12(a), the traditional PI controller performs the worst in terms of recovery time and disturbance rejection capability. In contrast, the improved LADRC can compensate for the voltage drop faster, successfully achieving stronger robustness.

C. ROBUSTNESS UNDER GRID VOLTAGE SAG

Finally, the voltage regulation operation was tested in the PV grid-connected system to evaluate the feasibility of the improved LADRC scheme in abnormal conditions (such as grid voltage sag). Grid operation criteria require PV power generation system to keep grid-connected for a while during grid voltage sag.

Fig. 13 presents the DC-link voltage waveform when a three-phase balance drop fault occurs in the grid voltage under nominal operating conditions. The disturbance rejection capability can be demonstrated through the maximum voltage fluctuation Δu and the recovery time Δt. In dealing with different degrees of grid voltage sag, the three control schemes all show similar behaviors, which can restore the DC-link voltage to a stable state after encountering disturbances. However, as the fault deepens, the grid-connected inverter exhibits a worse disturbance rejection capability, which can be explained by the increase in Δu and Δt. Especially for the plant employing the PI controller, the Δu and Δt vary widely under different sag conditions. Also, the two indicators based on PI control under the same operating conditions are much larger than those using LADRC or its improved one. Therefore, the plant using PI controller does not have strong robustness. Furthermore, the inverter based on the improved LADRC exhibits superior a higher level of control performance under various operating conditions, both in terms of Δu and Δt, in comparison to the conventional LADRC.

The above experimental results also match the theoretical analysis in Section IV.

VI. CONCLUSION

In the PV grid-connected system, the robust control of DC-link voltage is crucial for energy transmission, which directly affects the power quality. Therefore, a DC-link voltage control strategy based on improved LADRC was proposed for grid-connected inverter in this paper. By describing the stability problem and power relationship of the DC-link, the voltage outer loop is modeled. Both theoretical analysis and experimental results prove that the proposed voltage control scheme achieves better control performance, either during the start-up process or operating conditions variation. The reason is that the D-LESO established according to the principle of deviation regulation can estimate the total disturbance in a relatively timely and accurate manner, which lays a foundation for disturbance compensation.

At present, an increasing number of scholars are focusing their research on the combination of LADRC and intelligent algorithms, such as neural networks and fuzzy control. This paper is expected to provide these scholars with more ideas in order to apply LADRC more widely in the industrial field.

APPENDIX

The total disturbance estimation transfer function of LESO:

$$\frac{z_2}{f} = \frac{\omega_o^2}{(s+\omega_o)^2}$$

Transfer function of system output with respect to input and total disturbance:

$$y = \frac{\omega_c^2 v}{(s+\omega_c)^2} + \frac{s(s+2\omega_c+\omega_o)f}{(s+\omega_c)^2(s+\omega_o)^2}$$

Coefficients of characteristic polynomials (31) of closed-loop systems based on improved LADRC:

$$\begin{aligned} p_0 &= 8C_2Tb_0u_{dc}^* \\ p_1 &= 2b_0C_2u_{dc}^*(1+4\omega_oT+8\omega_cT)+3e_d\omega_o \\ p_2 &= 2b_0C_2u_{dc}^*(\omega_o+2\omega_c)+3e_d(\omega_o^2+4\omega_o\omega_c+\omega_c^2) \\ p_3 &= 6e_d\omega_o\omega_c(\omega_o+\omega_c), \quad p_4 = 3\omega_o^2\omega_c^2e_d \end{aligned}$$

REFERENCES

[1] A. Demirbas, "Global renewable energy projections," *Energy Sources, B, Econ., Planning, Policy*, vol. 4, no. 2, pp. 212–224, Oct. 2009.

[2] B. Yang, W. Li, Y. Zhao, and X. He, "Design and analysis of a grid-connected photovoltaic power system," *IEEE Trans. Power Electron.*, vol. 25, no. 4, pp. 992–1000, Apr. 2010.

[3] E. Romero-Cadaval, B. Francois, M. Malinowski, and Q.-C. Zhong, "Grid-connected photovoltaic plants: An alternative energy source, replacing conventional sources," *IEEE Ind. Electron. Mag.*, vol. 9, no. 1, pp. 18–32, Mar. 2015.

[4] L. Hassaine, E. OLias, J. Quintero, and V. Salas, "Overview of power inverter topologies and control structures for grid connected photovoltaic systems," *Renew. Sustain. Energy Rev.*, vol. 30, pp. 796–807, Feb. 2014.

[5] B. Guo, S. Bacha, M. Alamir, and H. Iman-Eini, "A robust LESO-based DC-link voltage controller for variable speed hydro-electric plants," in *Proc. IEEE Int. Conf. Ind. Technol. (ICIT)*, Feb. 2019, pp. 361–366.

[6] M. Coppola, F. Di Napoli, P. Guerriero, D. Iannuzzi, S. Daliento, and A. D. Pizzo, "An FPGA-based advanced control strategy of a grid-tied PV CHB inverter," *IEEE Trans. Power Electron.*, vol. 31, no. 1, pp. 806–816, Jan. 2016.

[7] R. Chinnappan, P. Logamani, and R. Ramasubbu, "Fixed frequency integral sliding-mode current-controlled MPPT boost converter for two-stage PV generation system," *IET Circuits, Devices Syst.*, vol. 13, no. 6, pp. 793–805, Sep. 2019.

[8] D. Chen, L. Xu, and L. Yao, "DC voltage variation based autonomous control of DC microgrids," *IEEE Trans. Power Del.*, vol. 28, no. 2, pp. 637–648, Apr. 2013.

[9] J. L. Sosa, M. Castilla, J. Miret, J. Matas, and Y. A. Al-Turki, "Control strategy to maximize the power capability of PV three-phase inverters during voltage sags," *IEEE Trans. Power Electron.*, vol. 31, no. 4, pp. 3314–3323, Apr. 2016.

[10] J. Du, H. Zhao, and H. Sun, "Outer loop voltage control method based on DC power control of three-phase grid-connected inverter," *Acta Energiae Solaris Sinica.*, vol. 40, no. 9, Sep. 2019.

[11] B. N. Singh, P. Jain, and G. Joos, "Three-phase AC/DC regulated power supplies: A comparative evaluation of different topologies," in *Proc. 15th Annu. IEEE Appl. Power Electron. Conf. Expo. (APEC)*, vol. 1, Feb. 2000, pp. 513–518.

[12] J. F. Silva, "Sliding-mode control of boost-type unity-power-factor PWM rectifiers," *IEEE Trans. Ind. Electron.*, vol. 46, no. 3, pp. 594–603, Jun. 1999.
[13] J. G. Hwang and P. W. Lehn, "A single-input space vector for control of AC–DC converters under generalized unbalanced operating conditions," *IEEE Trans. Power Electron.*, vol. 25, no. 8, pp. 2068–2081, Aug. 2010.
[14] J. Chen, R. J. Patton, and H.-Y. Zhang, "Design of unknown input observers and robust fault detection filters," *Int. J. Control*, vol. 63, no. 1, pp. 85–105, Jan. 1996.
[15] W.-H. Chen, J. Yang, L. Guo, and S. Li, "Disturbance-observer-based control and related methods—An overview," *IEEE Trans. Ind. Electron.*, vol. 63, no. 2, pp. 1083–1095, Feb. 2016.
[16] R. Madoński and P. Herman, "Survey on methods of increasing the efficiency of extended state disturbance observers," *ISA Trans.*, vol. 56, pp. 18–27, May 2015.
[17] Y. Huang and W. Xue, "Active disturbance rejection control: Methodology and theoretical analysis," *ISA Trans.*, vol. 53, no. 4, pp. 963–976, Jul. 2014.
[18] J. Han, "From PID to active disturbance rejection control," *IEEE Trans. Ind. Electron.*, vol. 56, no. 3, pp. 900–906, Mar. 2009.
[19] Z. Gao, "Scaling and bandwidth-parameterization based controller tuning," in *Proc. Amer. Control Conf.*, 2003, pp. 4989–4996.
[20] H. Sira-Ramírez, J. Linares-Flores, C. García-Rodríguez, and M. A. Contreras-Ordaz, "On the control of the permanent magnet synchronous motor: An active disturbance rejection control approach," *IEEE Trans. Control Syst. Technol.*, vol. 22, no. 5, pp. 2056–2063, Sep. 2014.
[21] W. Xue and Y. Huang, "Performance analysis of active disturbance rejection tracking control for a class of uncertain LTI systems," *ISA Trans.*, vol. 58, pp. 133–154, Sep. 2015.
[22] G. Tian and Z. Gao, "Frequency response analysis of active disturbance rejection based control system," in *Proc. IEEE Int. Conf. Control Appl.*, Oct. 2007, pp. 1595–1599, doi: 10.1109/CCA.2007.4389465.
[23] R. Yang, M. Sun, and Z. Chen, "Active disturbance rejection control on first-order plant," *J. Syst. Eng. Electron.*, vol. 22, no. 1, pp. 95–102, Feb. 2011.
[24] B. Guo, S. Bacha, M. Alamir, A. Mohamed, and C. Boudinet, "LADRC applied to variable speed micro-hydro plants: Experimental validation," *Control Eng. Pract.*, vol. 85, pp. 290–298, Apr. 2019.
[25] D. Yuan, X. J. Ma, Q.-H. Zeng, and X. Qiu, "Research on frequency-band characteristics and parameters configuration of linear active disturbance rejection control for second-order systems," *Control Theory Appl.*, vol. 30, no. 12, pp. 1630–1640, 2013.
[26] A. Benrabah, D. Xu, and Z. Gao, "Active disturbance rejection control of LCL-filtered grid-connected inverter using Padé approximation," *IEEE Trans. Ind. Appl.*, vol. 54, no. 6, pp. 6179–6189, Nov. 2018.
[27] G. Wang, R. Liu, N. Zhao, D. Ding, and D. Xu, "Enhanced linear ADRC strategy for HF pulse voltage signal injection-based sensorless IPMSM drives," *IEEE Trans. Power Electron.*, vol. 34, no. 1, pp. 514–525, Jan. 2019.
[28] K. Liu, J. He, Z. Luo, X. Shen, X. Liu, and T. Lu, "Secondary frequency control of isolated microgrid based on LADRC," *IEEE Access*, vol. 7, pp. 53454–53462, 2019.
[29] J. Lu, S. Golestan, M. Savaghebi, J. C. Vasquez, J. M. Guerrero, and A. Marzabal, "An enhanced state observer for DC-link voltage control of three-phase AC/DC converters," *IEEE Trans. Power Electron.*, vol. 33, no. 2, pp. 936–942, Feb. 2018.
[30] Y. Ma, X. Yang, X. Zhou, L. Yang, and Y. Zhou, "Dual closed-loop linear active disturbance rejection control of grid-side converter of permanent magnet direct-drive wind turbine," *Energies*, vol. 13, no. 5, p. 1090, Mar. 2020.
[31] S. N. Pawar, R. H. Chile, and B. M. Patre, "Modified reduced order observer based linear active disturbance rejection control for TITO systems," *ISA Trans.*, vol. 71, pp. 480–494, Nov. 2017.
[32] C. Liu, G. Luo, Z. Chen, W. Tu, and C. Qiu, "A linear ADRC-based robust high-dynamic double-loop servo system for aircraft electro-mechanical actuators," *Chin. J. Aeronaut.*, vol. 32, no. 9, pp. 2174–2187, Sep. 2019.

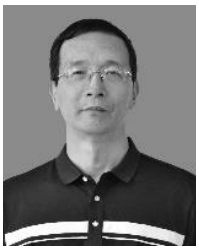

XUESONG ZHOU received the B.S. degree from the South China University of Technology, Guangzhou, China, in 1984, and the M.S. and Ph.D. degree from Tsinghua University, Beijing, China, in 1990 and 1993, respectively. From 1993 to 2002, he worked with the School of Electrical and Automation Engineering, Qingdao University, as the Deputy Dean and the Director of the Shandong Provincial Key Laboratory of Power Electronics Engineering. In 1996, he won the Guan Zhao-Zhi Award from the Chinese control industry. In 1997, he was promoted to a Full Professor. Since 2002, he has been working with the School of Electrical and Electronics, Tianjin University of Technology, as the Associate Dean and a Distinguished Professor of the school. His research interests include power system analysis and automation, smart grids, and the field of new energy utilization.

QIAN LIU was born in Hebei, China. He received the B.S. degree in electrical engineering from the North China University of Science and Technology, Tangshan, China, in 2019. He is currently pursuing the M.S. degree with the School of Electrical and Electronic Engineering, Tianjin University of Technology, Tianjin, China. His research interests include the application of active disturbance rejection control in grid-connected converters, renewable energy, and microgrids.

YOUJIE MA received the B.S., M.S., and Ph.D. degrees from Tsinghua University, Beijing, China, in 1987, 1990, and 1993, respectively. From 1993 to 2002, she worked with the School of Electrical and Automation Engineering, Qingdao University. In 1998, she was promoted to a Full Professor. Since 2002, she has been working as a Distinguished Professor with the School of Electrical and Electronic Engineering, Tianjin University of Technology, Tianjin, China. Her research interests include power system analysis and automation and smart grids.

BINGJIE XIE was born in Hebei, China. She received the B.S. degree in electrical engineering from the North China Electric Power University, Hebei, China, in 2019, where she is currently pursuing the M.S. degree in electrical and electronic engineering with the School, Tianjin University of Technology. Her current research interests include power electronics and PWM control technology.